

BarkBeetle: Stealing Decision Tree Models with Fault Injection

Qifan Wang
University of Birmingham
Birmingham, UK
q.wang.3@bham.ac.uk

Jonas Sander
University of Luebeck
Luebeck, Germany
j.sander@uni-luebeck.de

Minmin Jiang
Queen's University Belfast
Belfast, UK
m.jiang@qub.ac.uk

Thomas Eisenbarth
University of Luebeck
Luebeck, Germany
thomas.eisenbarth@uni-luebeck.de

David Oswald
University of Birmingham
Birmingham, UK
d.f.oswald@bham.ac.uk

Abstract

Machine learning models—particularly decision trees (DTs)—are widely adopted across various domains due to their interpretability and efficiency. However, as ML models become increasingly integrated into privacy-sensitive applications, concerns about their confidentiality have grown—particularly in light of emerging threats such as model extraction and fault injection attacks. Assessing the vulnerability of DTs under such attacks is therefore important. In this work, we present *BarkBeetle*, a novel attack that leverages fault injection to extract internal structural information of DT models. *BarkBeetle* employs a bottom-up recovery strategy that uses targeted fault injection at specific nodes to efficiently infer feature splits and threshold values. Our proof-of-concept implementation demonstrates that *BarkBeetle* requires significantly fewer queries and recovers more structural information compared to prior approaches, when evaluated on DTs trained with public UCI datasets. To validate its practical feasibility, we implement *BarkBeetle* on a Raspberry Pi RP2350 board and perform fault injections using the Faultier voltage glitching tool. As *BarkBeetle* targets general DT models, we also provide an in-depth discussion on its applicability to a broader range of tree-based applications, including data stream classification, DT variants, and cryptography schemes.

Keywords

Fault injection attack, decision tree, model extraction attack

1 Introduction

Recent advancements in Machine Learning (ML), particularly in Decision Tree (DT) models, have driven significant progress across a variety of applications. Due to their strong interpretability, DTs are widely adopted in areas such as online health diagnostics and data stream mining [12, 37]. To further facilitate ML deployment, cloud-based platforms such as Amazon, Google, Microsoft, and BigML have emerged, offering Machine Learning as a Service (MLaaS) Application Programming Interface (API) for model training and inference. At the same time, ML is increasingly supported on embedded devices. Platforms from Arduino, Adafruit, and STMicroelectronics support lightweight ML frameworks such as TensorFlow Lite for Microcontrollers [10], Edge Impulse [21], and Emlearn [31], enabling inference on resource-constrained devices. In privacy-sensitive fields such as healthcare and fraud detection, the models themselves may contain proprietary or sensitive information, potentially revealing secret information about the training data or

model's structure. Preserving the confidentiality of ML models is therefore essential, as unauthorized extraction or replication can allow adversaries to bypass detection mechanisms or cause critical failures, particularly in high-stakes applications like medical decision-making.

Recently, the increasing commercialization of ML services and growing reliance on third-party models have introduced new security and privacy concerns for organizations. Among these, inference attacks—such as membership inference [36], model inversion [14], and model extraction [39]—pose significant threats. Particularly, model extraction (or say stealing) attacks, first introduced by Tramèr et al. [39], target MLaaS platforms with the aim of reconstructing proprietary models. Following this seminal work, substantial research has been devoted to model extraction, especially for Neural Network (NN) models [7, 20, 22, 25, 43], where attackers attempt to approximate the target model under various adversarial goals. The strongest form of such attacks seeks to replicate the functionality of the target model with near-identical behavior across all possible inputs. In contrast, only a limited number of studies have focused on extracting tree-based models [7, 32, 39]. These works typically rely on black-box access to the model's prediction interface and employ techniques such as identifying unique outputs, query synthesis via active learning, or the use of Explainable Artificial Intelligence (XAI) methods. However, these approaches often face limitations—including dependency on rich output information, high query complexity, and partial recovery of the model. For instance, extracting only decision boundaries while overlooking repeated feature usage within each path. This information offers deeper insights into the feature's relative importance, its influence on decision-making, and even the underlying distribution of the training data.

Another emerging area of interest involves the use of Fault Injection Attacks (FIAs) to induce faults in targeted regions of a model, with the aim of generating controlled erroneous outputs and, ultimately, revealing the model's structure or internal parameters. Prior research in this space has primarily focused on NN models, which can be broadly categorized into two types of attacks: misclassification [5, 18, 19, 26] and parameter recovery [6, 16, 35]. Misclassification attacks aim to degrade model accuracy by introducing minimal bit flips to the model parameters. In contrast, parameter recovery attacks seek to extract internal components of the model, such as weights and biases, particularly in the last layer. Despite the extensive attention given to NNs, the application of fault injection techniques to DT models remains unexplored—especially

in terms of extracting both structural and statistical information. In the context of misclassification, DTs are often more vulnerable to faults due to their simple and deterministic structure, which makes it easier for injected faults to significantly impact prediction accuracy. Furthermore, most existing works in FIAs have focused on theoretical feasibility, with limited realization of practical FIAs on devices.

Recently, DT models have demonstrated notable utility in various domains, including data stream classification [12], ensemble learning methods such as Gradient Boosted Decision Tree (GBDT) [15] and XGBoost [8], and cryptographic schemes [4, 28]. Given their increasing adoption in both performance-critical and security-sensitive applications, it is essential to assess the confidentiality of DTs under a range of adversarial threats—particularly model extraction and FIAs. Motivated by this gap, we propose *BarkBeetle*, a novel attack that integrates fault injection in the model extraction pipeline to effectively recover the full structure of a tree model. *BarkBeetle* performs a bottom-up reconstruction of the tree—recovering nodes from the leaves to the root. The attacker injects faults at specific internal nodes to manipulate branching behavior and observe resulting prediction labels. By selectively forcing the model to traverse left or right subtrees, the attacker can infer the features and thresholds used at each node. Our objective is to recover all internal nodes and associated decision tests (i.e., features and threshold values) across all paths of a DT, while minimizing the number of required queries.

1.1 Contributions

The key contributions of this work are summarized as follows:

- To the best of our knowledge, *BarkBeetle* is the first attack to apply fault injection for extracting decision tree models. As it targets general tree structures, *BarkBeetle* also provides a foundation for extending it to other widely used tree-based models in various settings (cf. Section 6).
- We design a bottom-up algorithm that leverages fault injection at target nodes to recover features and thresholds more efficiently. This approach reduces the number of required queries and is particularly effective for tree-based models, which share a hierarchical decision-making structure.
- We implement a proof-of-concept attack for *BarkBeetle* and show that *BarkBeetle* significantly reduces the number of queries compared to prior relevant work [39] on DTs trained with UCI datasets. In addition, *BarkBeetle* reveals more information, including duplicate features along each path, providing deeper insight into their influence and significance within the decision process.
- To demonstrate the practical feasibility of our attack, we evaluate *BarkBeetle* on a Raspberry Pi RP2350 board and implement the voltage glitch using the Faultier tool [17]. In our case study with a DT (depth 5, 11 leaves, trained on the Diabetes Diagnosis dataset), the attack required ~1,900 additional queries due to repeated glitch attempts. This overhead could be reduced by employing more precise fault injection techniques.

- To support reproducibility and future research, we will release the source code for *BarkBeetle* upon acceptance, enabling the development and evaluation of countermeasures. For the reviewers, an anonymised version is available at <https://anonymous.4open.science/r/BarkBeetle/>.

2 Background and Related Work

In this section, we first present the basics of DT models, followed by a summary of existing research on model extraction and FIAs in ML. Additionally, we introduce some commonly used FIA techniques.

2.1 Decision Tree

A DT consists of internal nodes and leaves, where each internal node is associated with a test on a feature, each branch represents the outcome of the test, and each leaf represents a label which is the decision taken after testing all the features on the corresponding path. The label value of the accessed leaf is the inference result.

The splits in a DT are determined by the features, which can be either continuous or categorical. Continuous features represent numerical values, such as *age* or *temperature*, and are split using threshold values (e.g., *age* < 50). In contrast, categorical features represent distinct classes (e.g., *color*) and are split based on categories (e.g., red and blue resulting in two branches).

Some ML prediction APIs, such as Amazon¹ and BigML², return information-rich outputs—specifically, high-precision *confidence scores* in addition to class labels. Specifically, each leaf is assigned both a class label and a confidence score. These prediction labels and confidence values can serve as unique identifiers for nodes, allowing an attacker to distinguish between leaves that share the same label, as demonstrated in [39].

2.1.1 Classification Tree and Regression Tree. A classification tree is typically used for categorical target labels, assigning inputs to predefined classes (e.g., “Yes” or “No” for predicting whether to play tennis). A regression tree, on the other hand, is designed for continuous labels, predicting numerical values such as house prices or temperatures. Instead of classifying, it partitions the data to minimize variance or mean squared error in the target variable within each group [34].

A key factor influencing DT extraction is the difference in output values between classification and regression trees. While classification trees predict discrete categories, regression trees output continuous values. As a result, different paths in a classification tree may lead to the same label, whereas all paths in a regression tree typically yield unique outputs. However, when multiple paths in a classification tree share the same label, it can reduce the attacker’s ability to distinguish between different paths (cf. Section 4.7.1).

2.2 Model Extraction Attack on ML Models

Model extraction attacks pose a serious threat to MLaaS platforms by stealing the functionality of private ML models through querying black-box APIs. Since the pioneering study by [39], research on these attacks has primarily focused on NN models [7, 20, 22, 25, 43]. These attacks consists of three key steps: i) generating queries,

¹<https://aws.amazon.com/machine-learning>

²<https://bigml.com/api/>

either sampled from the training dataset or synthesized; ii) sending each query to the MLaaS API and receiving its prediction result; iii) iteratively updating the stolen model using the query-response pairs [25]. Adversarial goals in model extraction attacks can be classified into three categories: i) *Functionally Equivalent Extraction*: The attacker creates a model that behaves identically, or nearly identically, to the target model for any input. ii) *Fidelity Extraction*: The attacker extracts a model that closely replicates the target model. While the extracted model may not be functionally identical, it aims to mimic the target model’s outputs with a high degree of accuracy. iii) *Task Accuracy Extraction*: The attacker extracts a model that matches or exceeds the target model’s accuracy. This goal is easier to achieve since the extracted model does not need to replicate the target model’s mistakes [22].

Only a few works [7, 32, 39] have studied extraction attacks on DT models. In [39], the authors initiate their attack by submitting a random input X , obtaining a leaf identifier, and subsequently identifying all constraints on X required to remain in that leaf. They iteratively generate new queries targeting previously unvisited leaves until the entire tree structure is identified. The number of queries can be significantly improved by employing incomplete queries—a functionality available through platforms like BigML—where certain input features are intentionally left unspecified. Specifically, the model traversal continues until an internal node with a split over a missing feature is reached, at which point the node’s threshold value is directly revealed. However, it can be easily mitigated by disabling it. The following work [7] relaxes assumptions regarding the availability of rich information, such as leaf identifiers and incomplete queries. Instead, they employ the IWAL algorithm introduced by [3], enabling DT extraction attacks without relying on auxiliary information. Finally, their method requires more queries but achieves better accuracy on DTs containing paths with the same labels. More recently, [32] exploits XAI to target interpretable models, aiming to infer decision boundaries and create surrogate models. Their experimental results demonstrate significantly greater efficiency compared to the prior two studies. However, it strongly depends on the availability of rich information provided by the MLaaS platform—information that may not always be accessible and could be restricted. Moreover, some of this rich information is part of the attack objectives in DT extraction.

Overall, these existing approaches suffer from one or more of the following limitations: ❶ reliance on rich auxiliary information; ❷ requiring a large number of queries; ❸ recovering only the decision boundaries of features in each tree path while overlooking the feature importance within each path (i.e., repeated feature usage within each path). Specifically, if a feature appears multiple times along a path, it reflects not only its overall importance but also its conditional relevance—its continued predictive relevance following earlier splits. This pattern can also offer insights into the underlying distribution of the training data [27].

2.3 Fault Injection Attack on ML Models

FIAs aim to manipulate a system’s behavior or extract sensitive data by intentionally introducing faults. In this section, we provide an overview of commonly used FIA techniques and summarize existing research on FIAs in ML.

2.3.1 Fault Injection Methods. Fault injection can be performed using various techniques and equipment, depending on factors such as the number of fault injection events, the fault location, timing, the number of affected bits, the duration of the fault, the types of gates targeted, and the nature of the fault [2, 38].

Clock/voltage glitch. Voltage glitching is achieved by momentarily dropping the supply voltage during specific operations, while clock glitching disrupts clock timing to violate the hardware’s setup and hold requirements, typically by inserting glitch pulses between normal clock cycles.

Electro-Magnetic (EM) fault injection. An EM fault injection involves generating a localized, short-duration, high-intensity electromagnetic pulse, inducing unintended currents in the chip’s internal circuitry.

Optical fault injection. This method uses equipment with varying precision, ranging from camera flashes to lasers. It offers high reproducibility and precision, with lasers capable of inducing exact bit flips.

Rowhammer. The Rowhammer attack is a software-based fault injection technique that can be triggered remotely. By repeatedly accessing one memory row, interference with neighboring rows can occur due to the dense memory structure, causing faster charge leakage. If the refresh rate is insufficient, bit flips may occur.

Since voltage glitches can be fine-tuned to target specific timing in the execution cycle, allowing precise disruption of specific operations, and are low-cost compared to advanced fault injection methods like laser or optical techniques, we focus on using the voltage glitch method to induce faults in this work (cf. detailed experiment setup in Section 5.4).

2.3.2 Fault Injection Attacks on ML Models. Over the past few decades, extensive research has been conducted on FIAs targeting ML models, particularly NNs. We summarize this line of research in two main categories based on their attack goals: namely *misclassification* and *parameter recovery*. In misclassification-based studies [5, 18, 19, 26], the goal is to reduce the model’s accuracy drastically by introducing as few faulty bits as possible into the target NN’s parameters. For example, [18] examined the effects of bitwise corruptions on 19 Deep Neural Network (DNN) models across six architectures and three image classification tasks. They found that factors such as the bit-flip position, flip direction, parameter sign, and layer width have a significant impact on the extent of the accuracy degradation.

In parameter recovery-based studies [6, 16, 35], the objective is to partly recover NN parameters, such as the weights and biases in the last layer. For instance, [18] employed the Rowhammer attack to recover significant bits (from LSB to MSB) and train a substitute model. [16] extended this approach to a 32-bit microcontroller, recovering over 90% of the most significant bits using around 1500 crafted inputs, allowing them to train a near-equivalent model.

Despite extensive research on fault injection in NNs, no existing studies have explored the use of FIAs to extract both the structural and statistical information of DT models. In terms of misclassification in DT models, this is likely because the structural characteristics of DTs make it relatively easy to induce faults which can significantly degrade the model accuracy compared to NNs. In this

work, we explore FIAs in DT models with the goal of extracting (or say recovering) both their structural and statistical information.

3 Data and Model Representation

Table 1: Notations used in this paper.

Notation	Description
d	Number of features
X	Data sample where $ X = d$ and $X = (x_0, x_1, \dots, x_{d-1})$
S	Feature set, $S = (s_0, s_1, \dots, s_{d-1})$
V	Tree node, $V = (s, t, br)$ where s, t , and br denote the feature, threshold values, and edge direction in this node
L	Labels in tree leafs, $L = (c_0, c_1, \dots, c_{\alpha-1})$
P	Tree path, $P = \{(V_0, V_1, \dots, V_{\beta-1}), c\}$ contains β nodes on the path and label
Y	Tree, comprised of α tree paths $(P_0, P_1, \dots, P_{\alpha-1})$
t_i^j	Threshold in the j -th (from the leaf to the root) duplicated node for feature s_i
Algorithms	
F_Inf()	Algorithm 1: Fault-based Inference (Normal inference is denoted as Inf())
FaBS()	Algorithm 2: Fault-assisted Binary Search
FFD()	Algorithm 3: First Feature Discovery
DFD()	Algorithm 4: Duplicate Features Discovery
RTI()	Algorithm 5: Recover Tree Iterator
TreeExt()	Algorithm 6: DT Extraction

In this section, we present the formal representations for query data array and DT model. In the rest of this paper, we use notations listed in Table 1.

3.1 Data Representation

In *BarkBeetle*, we primarily focus on continuous features, as they are more prevalent in common DT models. Moreover, categorical features can be more easily identified by systematically adjusting their values and observing the corresponding label changes.

$S = (s_0, s_1, \dots, s_{d-1})$ represents a set of d continuous features with the range $s_i \in [a, b]$. The minimal and maximal values of feature s_i are denoted as $s_i.a$ and $s_i.b$ respectively. A non-labeled query data is denoted as $X = (x_0, x_1, \dots, x_{d-1})$. As in prior work [39], we assume that the range $[a, b]$ can be inferred from the background information. For instance, if a DT has been deployed and actively used over time, an attacker can estimate $[a, b]$ for each feature by analyzing historical query patterns and responses.

3.2 Model Representation

Formally, we assume that each internal node is assigned a feature $s_i \in S$ and a binary splitting function, i.e., $x_i < t_i$, where x_i is the value of the i -th feature s_i in the given data sample and t_i is the threshold value for the i -th feature in this node determined during training. A tree Y consists of a set of paths $(P_0, P_1, \dots, P_{\alpha-1})$, where α is the number of paths in the tree. Each tree path $P = (V_0, V_1, \dots, V_{\beta-1}, c)$ contains β internal nodes, namely $V = (s, t)$, and the corresponding label c . Without loss of generality, we introduce an auxiliary attribute br , to indicate the direction of the edge: $br = 0$ indicates that the next node is its left child, while $br = 1$ signifies the right child. This attribute br is essential for crafting inputs that lead to different labels in our attack (cf. Algorithm 5). Finally, we represent a node as $V = (s, t, br)$. Note that a feature may appear

multiple times within the same path or across different paths, as a continuous feature can be split multiple times in the tree. The labels in the leafs of the DT are represented as $L = (c_0, c_1, \dots, c_{\alpha-1})$.

Given an input $X = (x_0, x_1, \dots, x_{d-1})$, the DT-inference proceeds as follows: Starting at the root, when an internal node V is reached, the split function $x_i < V.t$ is evaluated. If $x_i < V.t$, the process moves to the left child; otherwise, it moves to the right child. Once a leaf node is reached, the inference process terminates, and the label stored in the leaf is returned as the result. We assume that each leaf node has a unique identifier (e.g., label). This is also the reason why [39] and *BarkBeetle* perform better on regression trees, where each output is a distinct real value, making it easier to use as a unique identifier. For a discussion on how this restriction can be relaxed, please refer to Section 4.7.1.

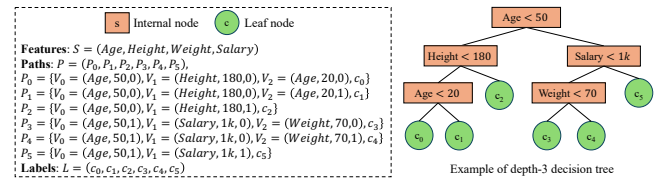


Figure 1: Representation of a toy DT model.

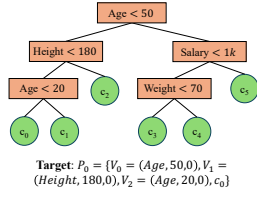
We provide a toy example of a depth-3 DT in Figure 1. Based on our data and model representations, the tree can be represented as feature set S , path set P , and label set L .

4 Methodology

In this section, we begin by presenting the threat model, outlining the attack objectives, capabilities, and knowledge assumed for the adversary in *BarkBeetle*. We then introduce the building blocks of our attack, explaining the types of faults used in DT inference. Next, we describe how *BarkBeetle* recovers feature and threshold values by first identifying the initial occurrence of each feature on a path (3), followed by detecting and recovering duplicate features along the same path (4). To aid understanding, Figure 2 provides a step-by-step example aligned with Figure 1, illustrating the entire recovery process and how each component fits together. Finally, we discuss how certain assumptions can be relaxed and outline potential directions for improvement.

4.1 Threat Model

In this work, we consider the DT model Y , which is trained on a dataset and deployed for inference. We assume that Y is pre-trained, and any information from the training phase is beyond the scope of this study. Our work focuses on adversaries targeting DT models on embedded devices such as microcontrollers (e.g., Raspberry Pi RP2350 microcontroller used in our experiment, cf. Section 5.4.1). This choice is driven by *BarkBeetle*'s use of voltage glitching to induce fault injection, which is well-suited for embedded platforms. However, importantly, our attack is also applicable to cloud environments if the attacker can perform fault injection attacks within the cloud infrastructure (e.g., Rowhammer [30], undervolting [23, 29, 33], binary code modification [9], compiler-level fault injection [42], or debugger-based techniques [13]).



1. Discovering First Occurrence of Features (cf. Section 4.4, Algorithm 3, Figure 4)
 - i. Identify *Age* and *Height* on path P_0 by varying values to *min/max* in the query input;
 - ii. Confirm *Age* and *Height* appear at 0th and 1st nodes by injecting faults at each node to alter the branch outcome and subsequently observe label changes;
 - iii. Find *Age* is duplicated on this path since the labels are different after each fault injection;
 - iv. Confirm *Height* < 20 using binary search since *Height* is unique on this path.
2. Discovering Duplicate Features (cf. Section 4.5, Algorithm 4, Figure 5)
 - i. Given duplicate feature set $\{Age\}$, locate it at 2nd node;
 - ii. Confirm *Age* < 20 using binary search in a bottom-up manner;
 - iii. Apply **FaBS()** (cf. Section 4.3, Algorithm 2, Figure 3) to find the next *Age* threshold (*Age* < 50).

Figure 2: Walkthrough example of *BarkBeetle*, illustrating feature recovery steps based on Figure 1.

Attack goals. Our focus is on an attacker \mathcal{A} who aims to recover the tree structure and node information of Υ , i.e., *path set* P and *label set* L (see examples in Figure 1), in a DT-based inference system. We consider \mathcal{A} 's capabilities and knowledge regarding the victim model as follows:

Capabilities. First, \mathcal{A} has unlimited black-box access to query the model. Second, \mathcal{A} can induce controlled, transient faults at specific timing points by briefly varying the supply voltage beyond its nominal range. Third, \mathcal{A} can exploit measurable variations in the DT's inference time, allowing to infer the number of nodes along each path and estimate the execution windows of individual nodes at each internal node during each inference. The latter is required for precisely performing fault injection. Prior related work, such as [28], assumes that the faulted location of the tree node is arbitrary but known to the attacker. In this work, we assume that \mathcal{A} can leverage side channels, such as power or timing analysis, to extract this information.

However, if consider a weaker grey-box setting as in [16]—which is stronger than white-box setting [18, 35]) but weaker than black-box setting— \mathcal{A} may know the number of nodes in each path and the timing duration per node. This is common when the model structure is known, easy to infer, or partially revealed by earlier attacks. In such cases, \mathcal{A} does not require the third capability of leveraging timing variations.

Knowledge. In *BarkBeetle*, \mathcal{A} has no prior knowledge of the victim DT's structure and node information.

4.2 Fault-based DT Inference

We demonstrate how side-channel information is utilized to determine the necessary timing for inducing faults and then introduce the fault types required in *BarkBeetle*.

The attacker \mathcal{A} requires timing information to inject faults at specific tree nodes. We assume that \mathcal{A} can exploit side-channel leakage to estimate the start and end times of each node's execution—denoted as $\mathcal{T}[i][0]$ and $\mathcal{T}[i][1]$ for the i -th node—via a procedure $P, \mathcal{T} \leftarrow \text{CTN}(\zeta_{sc}, P)$, where ζ_{sc} represents the observed side-channel signals. This work is orthogonal to this attack.

The core idea of *BarkBeetle* is to manipulate the comparison result at a specific node, enabling the attacker to gradually infer the feature and threshold values on that path. 1 describes the types of faults required to achieve this. In general, *BarkBeetle* injects faults to control branch execution. Specifically, in the left subtree (i.e., the left partition of the root node), a fault is induced at a node to force the branch to go left, regardless of the original decision. For example, given the comparison $x_0 < 20$ with a feature value

Algorithm 1 Fault-based Inference: $F_Inf()$

Input: Input X , timing array \mathcal{T} of P , target node index idx ; $flag = 0/1$ indicates left/right subtree
Output: Label c of faulted inference

```

1: if  $flag = 0$  then
2:   Flip comparison result of  $idx$ -th node to make it go left during  $[\mathcal{T}_{idx}[0], \mathcal{T}_{idx}[1]]$ 
3: else
4:   Flip comparison result of  $idx$ -th node to make it go right during  $[\mathcal{T}_{idx}[0], \mathcal{T}_{idx}[1]]$ 
5: end if
6:  $c \leftarrow Inf(X)$ 
```

Algorithm 2 Fault-assisted Binary Search: $FaBS()$

Input: Input X , baseline label c_b , timing array \mathcal{T} of P , feature index idx , node index $nidx$, low boundary low_bnd , high boundary $high_bnd$, flag $ifFIA$, left/right subtree flag $flag$, granularity ϵ
Output: Threshold value t

```

1:  $c_{ls} \leftarrow c_b$ ;  $low \leftarrow low\_bnd$ ;  $high \leftarrow high\_bnd$ 
2: while  $high - low \geq \epsilon$  do
3:    $X[idx] \leftarrow (low + high)/2$ 
4:   if  $ifFIA$  then
5:      $c_{ls} \leftarrow F\_Inf(X, \mathcal{T}, nidx, flag)$ 
6:   else
7:      $c_{ls} \leftarrow Inf(X)$ 
8:   end if
9:   if  $(flag = 0 \text{ and } c_{ls} = c_b) \text{ or } (flag = 1 \text{ and } c_{ls} = c_b)$  then
10:     $low \leftarrow X[idx]$ 
11:   else
12:     $high \leftarrow X[idx]$ 
13:   end if
14: end while
15:  $t \leftarrow X[idx]$ 
```

of $x_0 = 25$, the injected fault alters the expected execution flow, forcing the branch to take the left path instead of the originally intended right path. Conversely, in the right subtree, faults are applied to ensure the branch always goes right. Finally, \mathcal{A} obtains the label from fault-injected inference.

4.3 Fault-assisted Binary Search

In 2, our goal is to determine the threshold values for each feature. [39] employs *binary search* to identify the feature value range in which an input, while keeping all other feature values unchanged, leads to the same leaf node. However, this method failed to recover the repeated feature usage within each path. For example, consider a path with three nodes: $x < a$, $x < b$, $x > c$ (where $a > b$). The approach in [39] would identify the range $c < x < b$ for feature x on this path while neglecting $x < a$. Our objective is to recover all threshold values, including those for duplicate features appearing at different nodes along the same path.

We propose a fault-assisted binary search, which consists of two types of searches: normal search and fault-assisted search. We use t_i^j to reference the threshold value in j -th (from the leaves to the root node) duplicated node regarding feature s_i . **Normal search:**

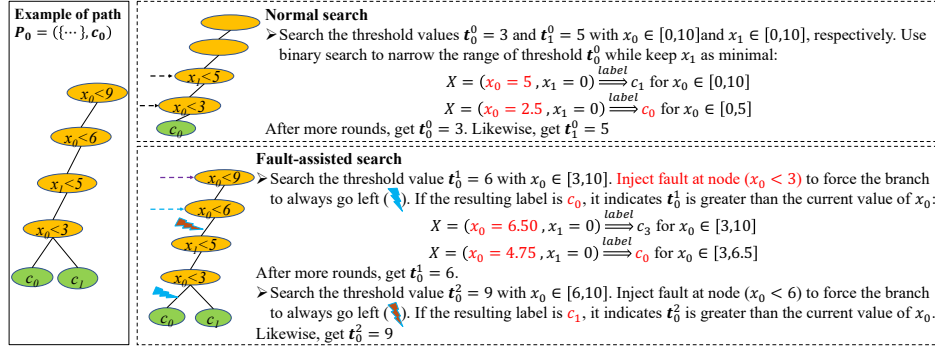


Figure 3: Illustration of fault-assisted binary search.

given lower and upper bounds, we apply binary search to determine the threshold t , ensuring that for any input satisfying $x_i < t$ (or $x_i > t$), the traversal leads to the existing leaf. As illustrated in Figure 3, we use binary search to progressively narrow the range of x_0 and determine the threshold $t_0^0 = 3$. **Fault-assisted search:** when duplicate features appear along the same path, injecting a fault at one node is insufficient. The key challenge is eliminating the influence of earlier nodes that also involve the same feature. To address this, we inject faults at the preceding node to manipulate branch execution and compare the resulting label with the baseline label (as detailed in 1). This allows us to extend the search range and accurately recover the next threshold value for the feature. For example, in Figure 3, we confirm the thresholds $t_1^0 = 6$ and $t_2^0 = 9$ for x_0 by injecting faults at earlier nodes (i.e., forcing the comparisons at $x_0 < 3$ and $x_0 < 6$ to always branch left, respectively).

4.4 Discovering First Occurrence of Features

Algorithm 3 First Feature Discovery: FFD()

Input: Path P , input X , timing array \mathcal{T} of P , left/right subtree flag $flag$, duplicate feature candidate set S_{DF} , granularity ϵ
Output: Updated P and S_{DF}

```

1: Initialize array  $S_{DF}$  which stores the duplicate features on path  $P$ 
2: for  $i = 0$  to  $d - 1$  do
3:    $X' \leftarrow X$ 
4:    $X'[i] \leftarrow (flag = 0) ? (s_i.b + 1) : (s_i.a - 1)$   $\triangleright$  Change a feature value to  $Min/Max$ 
5:    $P'.c \leftarrow \text{Inf}(X')$   $\triangleright i$ -th feature is on path  $P$  if  $P'.c \neq P.c$ 
6:    $P', T' \leftarrow \text{CTN}(\zeta_{sc}, P')$ 
7:   if  $P'.c \neq P.c$  then
8:     for  $j = 0$  to  $P'.\beta - 1$  do
9:        $c_f \leftarrow \text{F\_Inf}(X', T', j, flag)$ 
10:      if  $c_f \neq P'.c$  then  $\triangleright$  Indicate  $\text{F\_Inf}()$  alters the result of the  $i$ -th feature at  $j$ -th
node
11:         $P.V_j.s \leftarrow s_i$ 
12:        if  $c_f \neq P.c$  then  $\triangleright$  Indicate it traversed a new branch, thus  $s_i$  is duplicated
13:           $S_{DF}.append(s_i)$ 
14:        else
15:           $P.V_j.t \leftarrow \text{FABS}(X', P.c, \mathcal{T}, i, \text{None}, s_i.a, s_i.b, \text{False}, flag, \epsilon)$   $\triangleright$  Unique
feature  $s_i$ 
16:      end if
17:    end if
18:  end if
19: end for
20: end if
21: end for

```

Each path may contain both unique features (appearing only once) and duplicate features (appearing multiple times). Recovering duplicate features is inherently more complex than identifying

unique ones. In 3, we first recover the features that appear for the first time along a path. Overall, 3 can be summarized as two main steps: ❶ Modify each feature x_i to $s_i.b + 1$ (or $s_i.a - 1$ in the right subtree) while keeping all other feature values as $s_i.a - 1$, then check whether the label changes. For instance, in Figure 4, changing x_0 to $s_0.b + 1 = 11$ results in a label change to c_{16} , indicating that x_0 is present on this path. ❷ We then determine whether it appears once or multiple times. If it is a duplicate, we update the duplicate feature set S_{DF} , which will be processed in 4. For example, when changing x_1 to $s_1.b + 1$, in Figure 4, injecting a fault at the third node causes the label to change to c_0 , confirming that x_1 is present at this node as a unique feature, allowing us to determine its threshold value ($t_1^0 = 5$).

4.5 Discovering Duplicate Features

The primary challenge in recovering nodes with duplicate features along a path is also mitigating the influence of other nodes containing the same feature, as modifying the feature value can unintentionally lead to new paths, complicating the recovery process. 3 has already narrowed down the set of duplicate features. Building on this, we propose a bottom-up algorithm that reconstructs duplicate features from the last internal node to the root node. The key idea behind this bottom-up approach is to recover features starting from the smallest threshold (in the left subtree), thereby preventing interference from nodes that appear earlier in the path.

The process consists of three main steps: ❶ **Locating target node:** Given an already confirmed threshold, identify the node that contains this feature and threshold. To do this, modify $X[i]$ to $t_i \pm \epsilon$, ensuring that the modified input leads to a label different from the original label (say baseline label). Then, inject faults at each node and check whether the label changes to the baseline label. If so, the feature s_i with threshold t is confirmed at this node. For example, in the first round of Figure 5, after modifying x_2 to $t_0^0 + \epsilon = 4.01$, the label of the fault run matches the baseline label c_0 , confirming that $x_2 < 4$ belongs to the last node. ϵ represents the granularity used in the binary search. For features with large integer values, $t_i \pm \epsilon$ may have no effect. In such cases, ϵ should be experimentally tuned and replaced with a suitable value. ❷ **Updating feature value range and S_{DF} :** Narrow the feature value range and check if s_i appears in any remaining nodes. If not, remove it from S_{DF} to avoid redundant searches. ❸ **Searching for next threshold:** The

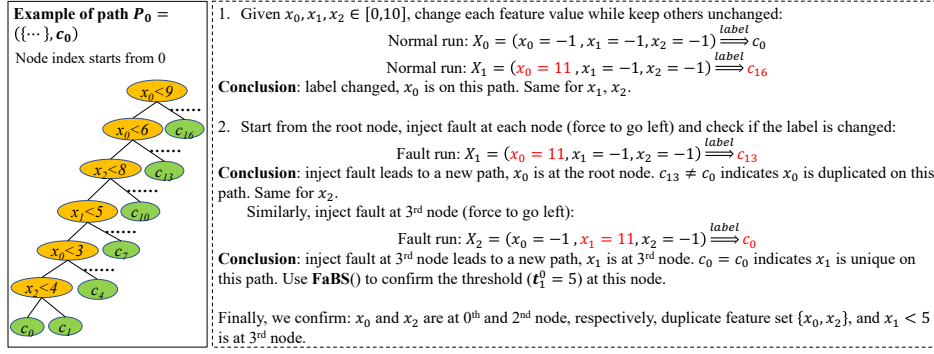


Figure 4: Example of FFD() for recovering the features first appear on this path.

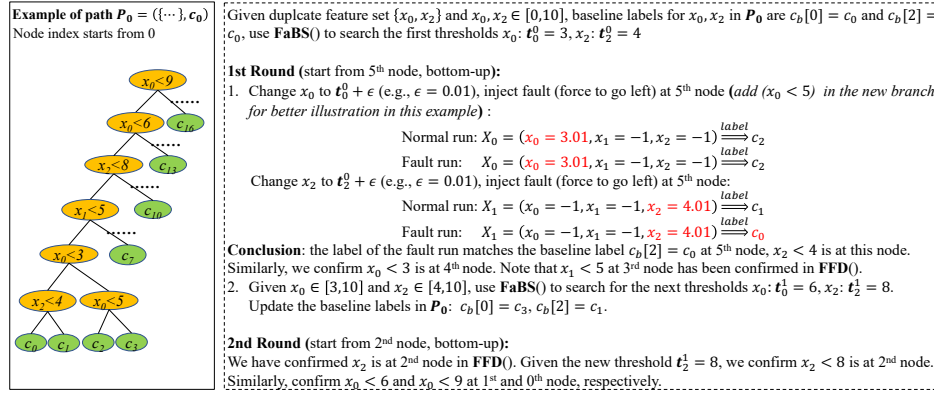


Figure 5: Example of DFD() for recovering duplicate features on this path.

next threshold for s_i is determined using **FaBS()**, and the baseline label for each duplicate feature is updated accordingly. For instance, in Figure 5, after confirming $x_2 < 4$ and $x_0 < 3$, the baseline labels for x_2 and x_0 are updated to c_1 and c_3 , respectively—representing the right-most labels for those nodes.

4.6 BarkBeetle

3 and 4 can be seen as the process of recovering a single tree path, while 5 and 6 serve as iterators to systematically reconstruct all paths in a DT. To iteratively recover paths based on previously recovered ones, a crucial step is generating new input arrays that will traverse along unexplored paths. Given j -th node (i.e., $x_i < t$), we modify $X[i]$ to $t \pm \epsilon$, ensuring that the modified input leads to a new label where branching occurs at the j -th node (Lines 13-19). As outlined in 6, the recovery process begins by selecting the leftmost and rightmost paths as the baseline, which are then used to systematically reconstruct all other extended paths.

4.7 Discussion

4.7.1 Different Paths with Identical Labels. As claimed in Section 3.2, we adopt the same assumption as [39], where each path (i.e., leaf) is assigned a unique identifier, allowing the attacker to distinguish between different tree paths by feeding the DT with customized

inputs. This assumption makes regression trees particularly well-suited for *BarkBeetle*, as each leaf node has a unique real-valued label. However, in classification trees, both [39] and *BarkBeetle* may fail to recover some paths if multiple paths share the same label. To address this limitation, we propose the following solutions for paths with:

Same label but different node counts. Under our threat model (cf. Section 4.1), *BarkBeetle* can distinguish such paths based on node counts, similar to [39].

Same label and same node counts. If an attacker has the capability to measure fine-grained timing variations, it may be possible to differentiate paths based on total inference time. The left and right branches at each node may introduce slight timing variations due to jump instructions, and if two paths follow different branching patterns, their overall execution time will differ, allowing for differentiation. However, if two paths not only share the same label and node count but also exhibit identical branching patterns (i.e., the same number of left and right branches), this approach becomes ineffective. A potential alternative is to leverage the confidence values associated with different leaves to distinguish them (cf. Section 2.1). However, this method may not be effective in all cases and requires further investigation.

Algorithm 4 Duplicate Features Discovery: DFD()

Input: Path P , input X , timing array \mathcal{T} of P , array fea_range records max/min value for each feature on this path, left/right subtree flag $flag$, duplicate feature array S_{DF} , granularity ϵ

Output: Updated P

```

1:  $tidx \leftarrow 0$  ▷ indicate the current threshold's index
2: Initialize arrays  $c_b$  and  $loc$  of size  $d$  which store the baseline label and node index for each feature, respectively
3: Initialize array  $t$  of size  $d \times h$  (depth  $h$ ), which stores each feature's previously confirmed threshold
4: for  $s_i \in S_{DF}$  do ▷ Search each duplicate feature's first threshold value (the one closest to the leaf)
5:    $c_b[i] \leftarrow P.c$ 
6:    $t[i][tidx] \leftarrow \text{FaBS}(X, c_b[i], \mathcal{T}, i, \text{None}, fea\_range[i][0], fea\_range[i][1], \text{False}, flag, \epsilon)$ 
7: end for
8: while not all  $P.V_j.t$  are recovered do
9:   for  $s_i \in S_{DF}$  do ▷ ❶ Identify the node containing the discovered threshold
10:     $X' \leftarrow X$ 
11:     $X'[i] \leftarrow (flag = 0) ? t[i][tidx] + \epsilon : t[i][tidx] - \epsilon$ 
12:    for  $j = P.\beta - 1$  to 0 do
13:      if  $P.V_j.t \neq \text{null}$  then
14:        continue ▷ Node is already recovered
15:      end if
16:      if  $P.V_j.s = s_i$  then
17:         $P.V_j.t \leftarrow \text{tres}[i][tidx]$ 
18:         $S_{DF}.\text{remove}(s_i)$  ▷ Last node containing  $s_i$  has been confirmed
19:        break
20:      end if
21:       $c_f \leftarrow \text{F\_Inf}(X', \mathcal{T}, j, flag)$ 
22:      if  $c_f = c_b$  then
23:         $P.V_j.s \leftarrow s_i$ 
24:         $P.V_j.t \leftarrow t[i][tidx]$ 
25:         $loc[i] \leftarrow j$  ▷ Record the index of the previous node including  $s_i$ 
26:        break
27:      end if
28:    end for
29:   end for
30:   for  $s_i \in S_{DF}$  do ▷ ❷ Update feature value range and check if  $s_i$  appears in the remaining nodes
31:      $fea\_range[i][flag] \leftarrow t[i][tidx]$ 
32:      $X'[i] \leftarrow (flag = 0) ? fea\_range[i][1] : fea\_range[i][0]$ 
33:      $c_{ifdup} \leftarrow \text{F\_Inf}(X', \mathcal{T}, loc[i], flag)$ 
34:     if  $c_{ifdup} = c_b[i]$  then
35:        $S_{DF}.\text{remove}(s_i)$  ▷  $s_i$  will not appear in the following nodes
36:     end if
37:   end for
38:   for  $s_i \in S_{DF}$  do ▷ ❸ Search for each duplicate feature's next threshold
39:      $t[i][tidx+1] \leftarrow \text{FaBS}(X, c_b[i], \mathcal{T}, i, loc[i], fea\_range[i][0], fea\_range[i][1], \text{True}, flag, \epsilon)$ 
40:      $X'[i] \leftarrow (flag = 0) ? t[i][tidx+1] - \epsilon : t[i][tidx+1] + \epsilon$ 
41:      $c_b[i] \leftarrow \text{Inf}(X')$ 
42:   end for
43:    $tidx++$ 
44: end while

```

4.7.2 Complexity Analysis. Since [39] is the most relevant work under similar assumptions, we compare *BarkBeetle* against it. Let m , d , h , and ϵ represent the number of leaves in the tree, the number of continuous features, the tree depth, and the granularity used in binary search, respectively, where $m = 2^{h-1}$. To analyze complexity, we adopt the same assumption that each leaf is assigned a unique identifier and that no continuous feature is split into intervals smaller than ϵ . For continuous features within the range $[0, b]$, determining a single threshold requires at most $\log_2 \frac{b}{\epsilon}$ queries. The complexity of [39] is $O(m^2 \cdot d \cdot \log_2 \frac{b}{\epsilon})$. For *BarkBeetle*, in the worst case (without distinguishing between unique and duplicate features), the complexity is $O(m \cdot (d + 2 \cdot d \cdot h + d \cdot \log_2 \frac{b}{\epsilon} + 2 \cdot d)) \approx O(m \cdot d \cdot (2h + \log_2 \frac{b}{\epsilon}))$. *BarkBeetle* achieves at least one order of magnitude improvement over [39]. Furthermore, *BarkBeetle* incurs different overheads when handling unique and duplicate features along each path (see Section 5.3 for breakdown benchmarks). As a result, when applied to real-world DT models, our performance is expected to be significantly better than the worst-case bound.

Algorithm 5 Recover Tree Iterator: RTI()

Input: All paths $(P_0, P_1, \dots, P_{\alpha-1})$ and their inputs \bar{X} of size $\alpha \times d$, left/right subtree flag LR_path for each P , array $paths_status$ tracking path discovery completion, array $start_node$ specifying recovery starting nodes, array $candidates$ selecting baseline paths for extending to news, granularity ϵ

Output: Updated $(P_0, P_1, \dots, P_{\alpha-1})$

```

1: for  $k = 0$  to  $\alpha - 1$  do
2:   if  $candidates[k] \neq 1$  then
3:     continue
4:   end if
5:   Initialize arrays  $t_{cur}$ ,  $br_{cur}$  of size  $d$  ▷ Record identified threshold and branch direction
6:   in  $P_k$ 
7:     for  $i \leftarrow start\_node[k]$  to  $P_k.\beta$  do
8:        $cur\_fea \leftarrow P_k.V_{i.s}; cur\_br \leftarrow P_k.V_{i.br}; cur\_t \leftarrow P_k.V_{i.t}$ 
9:       for  $j \leftarrow 0$  to  $i - 1$  do
10:        if  $P_k.V_{j.s} = cur\_fea$  then ▷ Record the nearest node containing feature
11:           $cur\_fea$ 
12:           $t_{cur}[cur\_fea] \leftarrow P_k.V_{j.t}; br_{cur}[cur\_fea] \leftarrow P_k.V_{j.br}$ 
13:        end if
14:      end for
15:      ▷ Modify  $cur\_fea$ -th feature value in  $\bar{X}[k]$  to traverse a new path branching at  $i$ -th node in  $P_k$ 
16:      if  $br_{cur}[cur\_fea] = \text{null}$  then ▷ Case: empty node
17:         $\bar{X}[k][cur\_fea] \leftarrow (cur\_br = 0) ? (cur\_t + \epsilon) : (cur\_t - \epsilon)$ 
18:      else if  $cur\_br = 0$  then ▷ Case: prev. branch is left/right and cur. is left
19:         $\bar{X}[k][cur\_fea] \leftarrow cur\_t + \epsilon$ 
20:      else if  $cur\_br = 1$  then ▷ Case: prev. branch is left/right and cur. is right
21:         $\bar{X}[k][cur\_fea] \leftarrow cur\_t - \epsilon$ 
22:      end if
23:       $c_m \leftarrow \text{Inf}(\bar{X}[k])$  where  $m \in (0, \alpha - 1)$ ;  $P_m, \mathcal{T}_m \leftarrow \text{CTN}(\zeta_{sc}, P_m)$ 
24:      Initialize  $fea\_range$  and  $S_{DF}$ 
25:      for  $j \leftarrow 0$  to  $P_m.\beta - 1$  do ▷ Copy the information of the same nodes into the new  $m$ -th path
26:        if  $j < i + 1$  then
27:           $P_m.V_{j.s} \leftarrow P_k.V_{j.s}$ 
28:           $P_m.V_{j.t} \leftarrow P_k.V_{j.t}$ 
29:           $P_m.V_{j.br} \leftarrow (j \neq i) ? P_k.V_{j.br} : (1 - P_k.V_{j.br})$ 
30:           $fea\_range[P_m.V_{j.s}][1 - P_m.V_{j.br}] \leftarrow P_m.V_{j.t}$ 
31:           $S_{DF}.\text{append}(P_m.V_{j.s})$ 
32:        else
33:           $P_m.V_{j.br} \leftarrow LR\_path[k]$ 
34:        end if
35:      end for
36:      for  $s_j \in S_{DF}$  do ▷ Check if the dup. feature will appear in the remaining nodes on this path
37:         $\bar{X}[k][j] \leftarrow (LR\_path[k] = 0) ? (fea\_range[j][1] - \epsilon) : (fea\_range[j][0] + \epsilon)$ 
38:         $c \leftarrow \text{Inf}(\bar{X}[k])$ 
39:        if  $c = c_m$  then
40:           $S_{DF}.\text{remove}(s_j)$ 
41:        end if
42:      end for
43:       $paths\_status[k] \leftarrow 0; LR\_path[m] \leftarrow LR\_path[k]$  ▷ Update auxiliary information for next loop
44:      if  $P_m.\beta = i + 1$  then
45:         $candidates[k] \leftarrow 0$ 
46:      end if
47:      continue
48:    end for
49:  end for

```

4.7.3 Stride-based Linear Search. As shown in Section 4.7.2, binary search constitutes a significant portion of the overhead. A potential alternative is to employ a stride-based linear search instead of relying solely on binary search in Algorithms 2, 3, and 4. Specifically, in the left subtree, the search begins at the lower bound, incrementally increasing the value by a *carefully chosen stride* to locate the threshold. In the right subtree, starting from the upper bound and decreasing by the same stride. This method avoids unnecessary searches from significantly larger bounds in binary search, reducing the number of queries required. However, the attacker must have an approximate understanding of the threshold distribution

Algorithm 6 DT Extraction: TreeExt()

Input: Features $S \leftarrow (s_0, s_1, \dots, s_{d-1})$
Output: Recovered tree \mathcal{Y}

- 1: Generate X_0 and $X_{\alpha-1}$, set $x_i \leftarrow s_{i,a-1}$ in X_0 and $x_i \leftarrow s_{i,b+1}$ in $X_{\alpha-1}$ for $i \in [0, d-1]$
- 2: Initialize baseline input array \bar{X} of size $\alpha \times d$, where each $\bar{X}[\cdot]$ represents an input designed to traverse a path
- 3: Initialize LR_path indicating whether each P is in the left or right subtree
- 4: Initialize $paths_status$, tracking completion of each path
- 5: Initialize $start_node$, the starting node index for recovery on each path
- 6: Initialize $candidates$, indicating which paths serve as baseline paths for extension in the loop
- 7: Initialize S_{DF} and fea_range where $fea_range[i][0] = s_{i,a}$ and $fea_range[i][1] = s_{i,b}$
- 8: Define granularity ϵ used in $FBS(\cdot)$, $FFD(\cdot)$, and $DFD(\cdot)$
- 9: **for** $i \in \{0, \alpha - 1\}$ **do** \triangleright Identify the leftmost/rightmost paths as baselines for extending new paths
- 10: $c_i \leftarrow \text{Inf}(X_i)$
- 11: $P_i, \mathcal{T}_i \leftarrow \text{CTN}(\zeta_{sc}, P_i)$
- 12: $FFD(P_i, X_i, \mathcal{T}_i, i, S_{DF}, \epsilon)$
- 13: $DFD(P_i, X_i, \mathcal{T}_i, fea_range, i, S_{DF}, \epsilon)$
- 14: $paths_status[i] \leftarrow 0$; $start_node[i] \leftarrow 1$; $candidates[i] \leftarrow 1$; $\bar{X}[i] \leftarrow X_i$;
 $LR_path[i] \leftarrow i$
- 15: **end for**
- 16: **while** $\text{Sum}(paths_status) \neq 0$ **do**
- 17: $\text{RTI}((P_0, P_1, \dots, P_{\alpha-1}), \bar{X}, LR_path, paths_status, start_node, candidates, \epsilon)$
- 18: **end while**
- 19: **return** $\mathcal{Y} \leftarrow (P_0, P_1, \dots, P_{\alpha-1})$

within the feature value range. A key challenge lies in selecting an appropriate stride size—if the stride is too large, it may skip over the correct threshold. One possible solution is to first perform a linear search with a moderate stride to identify a smaller range containing the threshold, followed by a binary search within this refined range for precise recovery. This approach is particularly beneficial for features with large value ranges, where binary search alone may be inefficient. We leave this interesting extension in future work.

5 Experiments

We implement a proof-of-concept attack for *BarkBeetle* in C, with a codebase of approximately 500 LoC. Using this implementation, we first compare *BarkBeetle* with prior work. Next, we provide a detailed performance breakdown of *BarkBeetle* across different metrics using customized flexible DTs. Finally, we describe our experimental setup for fault injection via voltage glitching and present the results of applying real glitch attack on DT.

5.1 Datasets and Models

To evaluate the performance of *BarkBeetle*, we utilize five commonly used datasets from the UCI Machine Learning Repository [1]. Detailed information about these datasets is provided in Table 2. For inference, we deploy DT models on embedded devices. These models are generated using ML library, Emlearn [31], that supports microcontrollers and embedded systems. Emlearn allows models to be trained in Python and then converted into a C classifier, enabling efficient inference on any device equipped with a C99 compiler.

5.2 Comparison of *BarkBeetle* and Prior Work

As discussed in Section 2.2, only a few studies [7, 32, 39] have explored model extraction attacks on DT models. [7] formulates model extraction as query synthesis active learning. Their approach generally requires significantly more queries than [39], but achieves higher accuracy. Moreover, their results are currently not publicly available for reproduction. [32] leverages XAI technique for extracting DT models. However, their method relies on rich auxiliary

information, such as feature importance, which is also an attack goal in *BarkBeetle*. Among these, [39] is the most relevant to *BarkBeetle*, making it the primary baseline for our comparison. In the following, we present a detailed comparison between *BarkBeetle* and [39].

Attack evaluation metric. To compare them, we primarily use the number of queries as the evaluation metric. We do not include accuracy as a comparison metric because both [39] and *BarkBeetle* reconstruct models that achieve the same accuracy as the original model. Specifically, we focus on models where each leaf (i.e., path) has a unique identifier, making regression trees the most suitable choice. In this scenario, *BarkBeetle* produces a model equivalent to the original as long as an appropriate ϵ is selected. For consistency, we use the same ϵ values as in [39] for different datasets in our experiments.

Testbed. Although we use the same UCI datasets as listed in [39], we do not directly report their published results. This is because, even when selecting the same datasets and tree depths, the total number of nodes and leaves in a BigML-generated tree cannot be controlled. Variations in tree structure ultimately lead to differences in the number of queries required for extraction. To ensure a fair comparison, we first generate DTs using the datasets listed in Table 2 through BigML’s online dashboard. We then convert the BigML-style tree into the Emlearn-compatible format. This transformation guarantees that the evaluated trees have an identical structure and number of nodes across experiments.

Since the code of [39] is no longer maintained and some dependencies have become outdated, we reconstructed their attack code within a Docker environment using compatible dependencies³. For running *BarkBeetle*, we use Ubuntu 24.04 on a Lenovo ThinkStation P2 Tower, equipped with 32 GB RAM and an Intel Core i7-14700 CPU (up to 5.30 GHz). The Docker container running [39]’s code is also executed on this machine.

Results. In our proof-of-concept attack for *BarkBeetle*, we report the total number of queries and the required fault runs in Table 2. For Iris and Diabetes Diagnosis, although these datasets correspond to classification trees with only two or three classes, the paths leading to the same class label contain different numbers of nodes, allowing the attacker to differentiate them. Note that we do not include results using the incomplete query functionality offered by BigML, as this feature is not commonly supported by other ML services. Moreover, this feature is overly powerful—reveals the node’s feature by feeding an incomplete query with the missing feature, making extraction much easier and less representative of real-world threat scenarios.

As expected in the complexity analysis (cf. Section 4.7.2), for smaller DTs such as Iris and Diabetes Diagnosis, *BarkBeetle* achieves only a slight improvement over [39] (e.g., 164 vs. 169 queries). However, for larger DTs, *BarkBeetle* requires significantly fewer queries (e.g., 4,092 vs. 11,460 queries). This gain is primarily due to *BarkBeetle*’s fault injection strategy that injects faults at target nodes and employs a bottom-up approach to iteratively refine the search space, minimizing unnecessary queries. Overall, *BarkBeetle* not only reduces query complexity but also extracts more information, such as the tree structure and duplicate features within a path, which are not recovered by prior methods.

³We will publicly release this Docker image to facilitate reproducibility.

Table 2: Performance of *BarkBeetle* on public models. For each model, we report the number of features used in this model, the number of classes (\mathbb{R} represents this tree is the regression tree), the number of leaves (i.e., paths), the maximum tree depth, and ϵ denotes the chosen granularity.

Model	# Features	# Classes	# Leaves	Depth	ϵ	# Queries		
						[39]	Ours Total	Fault Runs
Iris	3	3	9	5	10^{-3}	169	164	45
Diabetes Diagnosis	5	2	11	5	10^{-3}	256	248	29
Medical Provider Charge	11	\mathbb{R}	50	10	10^{-3}	2,541	1,718	311
Bitcoin Price	6	\mathbb{R}	147	11	10^{-4}	11,460	4,092	831
Appliances Energy Prediction	25	\mathbb{R}	158	17	10^{-3}	10,342	5,355	329

5.3 Evaluating *BarkBeetle* under Different Conditions

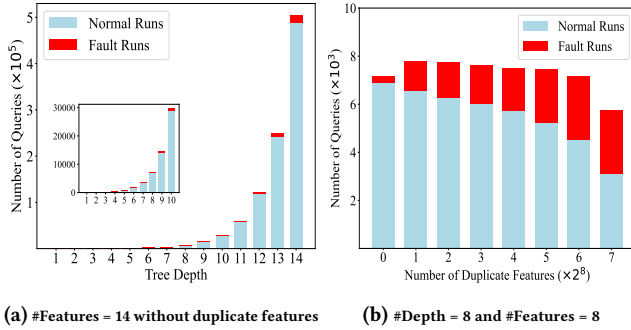


Figure 6: Performance of *BarkBeetle* under different tree depths (Figure 6a) and number of duplicate features (Figure 6b). $\epsilon = 10^{-3}$.

Based on the comparison with prior work, we identify tree depth and the number of duplicate features as two key factors that influence the number of queries required for model extraction. To systematically evaluate the impact of these factors, we assess the performance of *BarkBeetle* using synthetic DTs, which allow controlled variation in depth and feature duplication. These trees are generated using our custom Python script that produces complete binary trees with adjustable depth and numbers of duplicate features. The format of these trees is consistent with models generated by Emlearn.

In Figure 6a, we fix the number of features to 14 and vary the tree depth from 1 to 14, ensuring no duplicate features on any path. The results show that as tree depth increases, both the total number of queries and fault runs grow exponentially. For example, the number of queries increases from 401 at depth 4 to 833 at depth 5. This trend is expected, as deeper trees contain exponentially more internal nodes and decision paths.

In Figure 6b, we fix the tree depth to 8 and the number of features to 8, then increase the number of duplicate features from 0 to 7. We define duplicate features as follows: given depth h , a path with all h nodes using the same feature results in $h - 1$ duplicate features; a path with distinct features has 0 duplicates. Interestingly, the trend in Figure 6b does not follow a strictly increasing pattern. We observe the following: ❶ As the number of duplicate features increases, the

number of fault runs also rises, as expected, due to additional invocations of `DFD()`. However, the number of queries increases sharply when moving from 0 to 1 duplicate feature and then grows only gradually thereafter. This is because, once *BarkBeetle* invokes `DFD()` for the first time, new paths are extended from the baseline path. This allows some previously recovered nodes to be reused, avoiding redundant recovery efforts. Furthermore, as duplicate features increase, the search space for subsequent thresholds becomes narrower, contributing to reduced query overhead. ❷ When each path contains the maximum number of duplicate features (i.e., 7), the total number of queries is moderately lower than other cases. This further supports the above observation. In summary, these results highlight two key insights: ① In *BarkBeetle*, an increase in duplicate features leads to more fault runs, which may impact overall efficiency—particularly in real-world scenarios where each fault injection may require multiple attempts (cf. Section 5.4 for practical results). ② Despite the additional fault runs, the number of queries does not increase substantially with more duplicate features and, under certain conditions, may even decrease.

5.4 Results of Voltage Glitch-induced Faults in Inference

In this section, we demonstrate how practical faults can be induced in our proof-of-concept attack using voltage glitch, one of the most effective fault injection techniques.

5.4.1 Hardware Setup. Crowbar glitch mechanism. The glitching mechanism utilized in our setup is based on a crowbar circuit [41], which momentarily short-circuits the power rails of the target device (top-right corner of Figure 7a). The resulting glitch waveform depends on the specific characteristics of the target’s power supply configuration.

Glitch tool. For the voltage glitch attacks, we employ Faultier [17] to generate the required glitch waveforms. Faultier integrates an N-Channel MOSFET (DMG2302UK) for crowbar glitching and includes a dual-channel analog switch for performing voltage dips or re-powering the target device. In addition, Faultier provides a basic Serial Wire Debug (SWD) probe, allowing the extraction of memory contents from glitched chips and verifying the success of glitching by re-enabling debugging features. The tool supports glitch resolution up to 200 MHz (5 ns), offering fine-grained control over glitch timing. Figure 7a is an overview of all the components in Faultier ⁴.

⁴<https://app.hextree.io/>

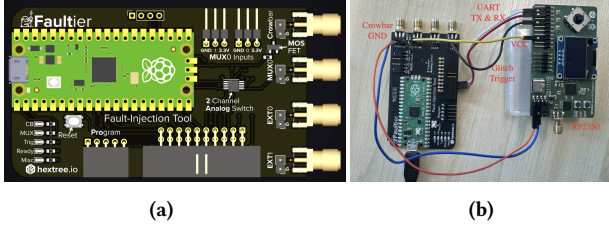


Figure 7: Overview of concept design of Faultier (Figure 7a) and hardware setup for the voltage glitching attacks (Figure 7b).

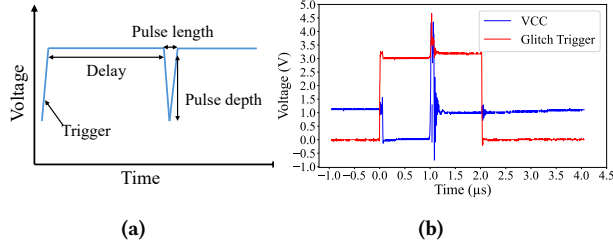


Figure 8: Glitch parameter conventions used in this experiment (Figure 8a) and waveforms for a successful glitch, including VCC and glitch trigger signals (Figure 8b).

Target device. We use the RP2350 Security Playground board, developed by the Faultier team, as shown in Figure 7b. This platform is specifically designed to evaluate fault injection resilience on RP2350-based systems. It includes built-in support for bypassing glitch detection and performing OTP fault testing, making it well-suited for practical security experiments. In our setup, we run DT inference on the board with security features like glitch detection deliberately turned off.

5.4.2 Signals during Fault Injections. As shown in Figure 8a, two key parameters define the glitch configuration: the glitch delay (delay), representing the time between the trigger signal and the glitch; and the glitch pulse length (pulse), indicating the duration of the glitch. During glitching attempts, we primarily adjust the (delay, pulse) pair (in cycle length) in Faultier to achieve successful fault injection on the target. Figure 8b shows the waveforms of a successful glitch at a target node, where the injected fault forces the branch to take the left path.

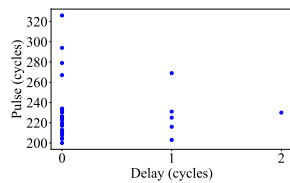


Figure 9: Successful glitch parameter pairs (i.e., (delay, pulse)).

5.4.3 Glitch Results for Inference. To evaluate our attack with the voltage glitch, we fine-tune the glitch parameter pair to induce the

desired fault type (e.g., forcing the branch to go left or right). Accordingly, we focus on the fault runs reported in Table 2, using the tree trained on the Diabetes Diagnosis dataset as a representative example. For each of the 29 fault runs, we record the first successful (delay, pulse) pair that induces a valid fault, with results presented in Section 9. The glitching process involves gradually increasing both delay and pulse values from zero while monitoring the system response to detect a successful injection. In principle, we can define large search ranges—e.g., $\text{delay} \in [0, 1000]$ and $\text{pulse} \in [0, 500]$ (as done in Faultier’s tutorials [17])—to ensure the space includes at least one successful pair. However, a more efficient strategy is to first perform offline glitching on a structurally similar tree to identify a viable glitch pair for each node. Based on this empirical knowledge, we can significantly narrow the search range when faulting one node. For example, given a successful glitch pair (1, 224), we can restrict the search to $\text{delay} \in [1, 10]$ and $\text{pulse} \in [200, 250]$, thereby avoiding unnecessary attempts. In total, 703 extra runs were required—higher than in our idealized proof-of-concept—resulting in an overall execution time of approximately 70,994 cycles, say 0.53 ms at a 133 MHz CPU frequency. This overhead is expected due to the inherently probabilistic nature of voltage glitching and its limited precision. Nevertheless, in this evaluation, voltage glitching primarily serves as a practical demonstration of our attack methodology. We believe that employing more precise and controllable fault injection techniques—such as EM or laser-based methods—could significantly reduce the gap between the real-world performance of *BarkBeetle* and its ideal implementation.

6 Limitations and Discussions on More Use Cases

6.1 Limitations in Fault Injection Efficiency

As shown in Section 5.4, injecting faults at specific nodes via voltage glitching often requires multiple attempts for a single successful execution. In cases of improper setup or parameter tuning, the number of queries needed to recover the DT can increase significantly. To alleviate this, exploring alternative fault injection techniques for attacking DT models could be valuable. One potential approach is incorporating Rowhammer attacks into *BarkBeetle*, leveraging a hybrid offline-online workflow. For instance, when testing on a system equipped with a 4GB DDR3 DIMM memory subsystem in either single- or dual-channel configurations, [35] indicate that Rowhammer attacks targeting pages with at least one MSB bit offset require hammering approximately 3,000 rows per round, with an average execution time of 200 seconds. Approximately, considering the timing constraints of Rowhammer and *BarkBeetle*, a possible strategy is to pre-hammer target memory rows offline while ensuring the tree is loaded into the vulnerable memory area before the estimated success window. However, for newer DRAM architectures such as DDR5, achieving a successful fault injection may take considerably longer, introducing further challenges. Overall, investigating the feasibility and efficiency of alternative fault injection techniques within *BarkBeetle* remains an interesting direction for future research.

6.2 Countermeasures

As *BarkBeetle* integrates both model extraction and FIAs, countermeasures should be considered from each perspective. From the perspective of model extraction, differential privacy has been suggested as a defense mechanism in prior studies [32, 39]. However, typical strategies—such as adding noise to training data, employing static or dynamic output distortion, or perturbing feature importance scores—have demonstrated limited effectiveness against more sophisticated extraction methods. This underscores the necessity of investigating advanced, adaptive differential privacy solutions. From the perspective of fault injection, hardware-based protections such as voltage and clock monitoring circuits can detect abnormal operating conditions and initiate protective responses like system resets or entering a safe mode. Additionally, redundancy-based methods, such as duplicating critical computations combined with majority voting or result comparison, can detect discrepancies caused by faults, thereby reducing their impact.

6.3 Extension to Other Tree Variants

GBDT/XGBoost. GBDT [15] and its optimized variant, XGBoost [8], are ensemble learning methods that iteratively train shallow DTs, where each tree corrects the residual errors of the previous ones. Unlike traditional DTs, GBDT and XGBoost aggregate predictions from multiple trees using gradient-based optimization and regularization to improve accuracy and prevent overfitting. Due to this aggregation mechanism, directly applying *BarkBeetle* to recover individual nodes in GBDT/XGBoost is impractical, as only the final prediction is exposed. However, inspired by previous fault injection attacks—such as those on AES to infer the last-round key [40] and on NNs to extract weights and biases [6]—a similar approach can be explored. By strategically injecting faults at specific nodes and analyzing the resulting variations in the final output, it may be possible to reconstruct node parameters by leveraging the known output formula of GBDT/XGBoost.

Hoeffding tree in data stream classification. The Hoeffding Tree (HT), a variant of the DT, is widely used for data stream classification due to its ability to continuously and efficiently learn from incoming data [12]. Unlike traditional DTs, which are trained on static datasets, HTs are incrementally updated on-the-fly as new data arrives. A key characteristic of HT is that it can be queried at any time to provide a prediction. However, given the same input, the returned label may vary because the model dynamically evolves, with nodes being updated or even pruned based on a concept drift detector that identifies significant accuracy degradation. Applying *BarkBeetle* to HTs enables the recovery of modified nodes or subtrees. Since changes in the HT structure primarily reflect shifts in the data stream, a potential research direction is to explore whether these recovered components can help an attacker infer the underlying data distribution of the stream.

6.4 Tree-based Cryptographic Schemes

DTs have also found widespread use in cryptographic applications. For example, ZKFault [28] recently demonstrated that fault attacks on zero-knowledge-based post-quantum digital signature schemes can be devastating—allowing full secret key recovery in LESS and CROSS from a single fault injected into the seed tree. *BarkBeetle*

provides a complementary approach by physically injecting faults at specific nodes via voltage glitching. A promising future direction is to explore whether this targeted fault methodology can also compromise seed trees or other tree-based structures in cryptographic protocols, potentially revealing secret values.

For instance, function secret sharing (FSS) protocols such as distributed point functions (DPFs) [4] encode functions as binary trees split between multiple parties. If a fault is injected into one party’s decision path—e.g., flipping a comparison result—it may lead to selecting an incorrect leaf value (commonly used in *oblivious array access* [11]). Originally, a 2PC DPF protocol would return a_i (the i -th element of array a); after a fault, the result might become a_j . When this is explored in ML domains, the incorrect selection of a_j will lead to different labels (or say logits in NNs). It is interesting to investigate if we can leverage this indirect leakage to infer internal parameters of ML models.

Moreover, even privacy-preserving DT frameworks, such as those surveyed in [24], which use homomorphic encryption, secret sharing, or Trusted Execution Environments (TEEs), could be vulnerable to fault injection. For example, if a malicious client in such a system can inject transient faults into the model-serving enclave or MPC server and observe changes in the prediction results (as done in *BarkBeetle*), they may be able to infer the underlying tree structure or internal thresholds. This creates a new dimension of side-channel leakage that bypasses cryptographic protections and underscores the need for robust hardware-level fault countermeasures.

7 Conclusion

In this work, we introduce *BarkBeetle*, a novel model stealing attack that leverages fault injection to recover tree models. We design a bottom-up recovery algorithm combined with targeted fault injection at specific nodes, which significantly improves the efficiency of the search process for feature thresholds, thereby reducing the number of required queries. Our approach is capable of recovering all internal nodes and their corresponding threshold values. With a properly chosen search granularity ϵ , *BarkBeetle* can reconstruct a model that closely matches the original one. Through our proof-of-concept implementation, we demonstrate that *BarkBeetle* not only reduces query complexity compared to prior work but also recovers richer structural information. Additionally, we validate the practicality of our approach by deploying *BarkBeetle* on a microcontroller using the voltage glitch tool Faultier, successfully performing real-world fault injections to extract model parameters. Since *BarkBeetle* targets general DT models, it holds strong potential for broader applications. We further discuss its applicability to other domains, including popular tree-based models such as GBDT, XGBoost, and Hoeffding Trees, as well as tree-based cryptographic schemes.

References

- [1] Arthur Asuncion, David Newman, et al. 2007. UCI machine learning repository.
- [2] Hagai Bar-El, Hamid Choukri, David Naccache, Michael Tunstall, and Claire Whelan. 2006. The sorcerer’s apprentice guide to fault attacks. *Proc. IEEE* 94, 2 (2006), 370–382.
- [3] Alina Beygelzimer, Daniel J Hsu, John Langford, and Tong Zhang. 2010. Agnostic active learning without constraints. *Advances in neural information processing systems* 23 (2010).
- [4] Elette Boyle, Niv Gilboa, and Yuval Ishai. 2016. Function secret sharing: Improvements and extensions. In *Proceedings of the 2016 ACM SIGSAC conference*

- on computer and communications security. 1292–1303.
- [5] Jakub Breier, Xiaolu Hou, Dirmanto Jap, Lei Ma, Shivam Bhasin, and Yang Liu. 2018. Practical fault attack on deep neural networks. In *Proceedings of the 2018 ACM SIGSAC Conference on Computer and Communications Security*. 2204–2206.
 - [6] Jakub Breier, Dirmanto Jap, Xiaolu Hou, Shivam Bhasin, and Yang Liu. 2021. SNIFF: reverse engineering of neural networks with fault attacks. *IEEE Transactions on Reliability* 71, 4 (2021), 1527–1539.
 - [7] Varun Chandrasekaran, Kamalika Chaudhuri, Irene Giacomelli, Somesh Jha, and Songbai Yan. 2020. Exploring connections between active learning and model extraction. In *29th USENIX Security Symposium (USENIX Security 20)*. 1309–1326.
 - [8] Tianqi Chen and Carlos Guestrin. 2016. Xgboost: A scalable tree boosting system. In *Proceedings of the 22nd acm sigkdd international conference on knowledge discovery and data mining*. 785–794.
 - [9] Domenico Cotroneo, Anna Lanzaro, and Roberto Natella. 2016. Faultprog: Testing the accuracy of binary-level software fault injection. *IEEE Transactions on Dependable and Secure Computing* 15, 1 (2016), 40–53.
 - [10] Robert David, Song Han, Kevin Lai, Tri Huynh, Suyog Ravuri, Peter Anderson, Jonathan Johnson, Greg Yao, and Pete Warden. 2020. TensorFlow Lite Micro: Embedded Machine Learning on TinyML Systems. *arXiv preprint arXiv:2010.08678* (2020).
 - [11] Jack Doerner and Abhi Shelat. 2017. Scaling ORAM for secure computation. In *Proceedings of the 2017 ACM SIGSAC Conference on Computer and Communications Security*. 523–535.
 - [12] Pedro Domingos and Geoff Hulten. 2000. Mining high-speed data streams. In *Proceedings of the sixth ACM SIGKDD international conference on Knowledge discovery and data mining*. 71–80.
 - [13] Bo Fang, Karthik Pattabiraman, Matei Ripeanu, and Sudhanva Gurumurthi. 2014. GPU-Qin: A methodology for evaluating the error resilience of GPGPU applications. In *2014 IEEE International Symposium on Performance Analysis of Systems and Software (ISPASS)*. IEEE, 221–230.
 - [14] Matt Fredrikson, Somesh Jha, and Thomas Ristenpart. 2015. Model inversion attacks that exploit confidence information and basic countermeasures. In *Proceedings of the 22nd ACM SIGSAC conference on computer and communications security*. 1322–1333.
 - [15] Jerome H Friedman. 2001. Greedy function approximation: a gradient boosting machine. *Annals of statistics* (2001), 1189–1232.
 - [16] Kevin Hector, Pierre-Alain Moëlle, Jean-Max Dutertre, and Mathieu Dumont. 2023. Fault injection and safe-error attack for extraction of embedded neural network models. In *European Symposium on Research in Computer Security*. Springer, 644–664.
 - [17] Hextree.io. 2024. Faultier: Open-Source Fault Injection Tool. <https://github.com/hextreeio/faultier>
 - [18] Sanghyun Hong, Pietro Frigo, Yiğitcan Kaya, Cristiano Giuffrida, and Tudor Dumitras. 2019. Terminal brain damage: Exposing the graceless degradation in deep neural networks under hardware fault attacks. In *28th USENIX Security Symposium (USENIX Security 19)*. 497–514.
 - [19] Xiaolu Hou, Jakub Breier, Dirmanto Jap, Lei Ma, Shivam Bhasin, and Yang Liu. 2021. Physical security of deep learning on edge devices: Comprehensive evaluation of fault injection attack vectors. *Microelectronics Reliability* 120 (2021), 114116.
 - [20] Xing Hu, Ling Liang, Shuangchen Li, Lei Deng, Pengfei Zuo, Yu Ji, Xinfeng Xie, Yufei Ding, Chang Liu, Timothy Sherwood, et al. 2020. Deepsniffer: A dnn model extraction framework based on learning architectural hints. In *Proceedings of the Twenty-Fifth International Conference on Architectural Support for Programming Languages and Operating Systems*. 385–399.
 - [21] Shawn Hymel, Colby Banbury, Daniel Situnayake, Alex Elum, Carl Ward, Mat Kelcey, Mathijs Baaijens, Mateusz Majchrzycki, Jenny Plunkett, David Tischler, et al. 2022. Edge impulse: An mlps platform for tiny machine learning. *arXiv preprint arXiv:2212.03332* (2022).
 - [22] Matthew Jagielski, Nicholas Carlini, David Berthelot, Alex Kurakin, and Nicolas Papernot. 2020. High accuracy and high fidelity extraction of neural networks. In *29th USENIX security symposium (USENIX Security 20)*. 1345–1362.
 - [23] Zijo Kenjar, Tommaso Frassetto, David Gens, Michael Franz, and Ahmad-Reza Sadeghi. 2020. V0LTPwn: Attacking x86 Processor Integrity from Software. In *USENIX Security '20*. USENIX Association, Boston. <https://www.usenix.org/conference/usenixsecurity20/presentation/kenjar>
 - [24] Ágnes Kiss, Masoud Naderpour, Jian Liu, N Asokan, and Thomas Schneider. 2019. SoK: Modular and efficient private decision tree evaluation. *Proceedings on Privacy Enhancing Technologies* 2019, 2 (2019), 187–208.
 - [25] Jiacheng Liang, Ren Pang, Changjiang Li, and Ting Wang. 2024. Model extraction attacks revisited. In *Proceedings of the 19th ACM Asia Conference on Computer and Communications Security*. 1231–1245.
 - [26] Yannan Liu, Lingxiao Wei, Bo Luo, and Qiang Xu. 2017. Fault injection attack on deep neural network. In *2017 IEEE/ACM International Conference on Computer-Aided Design (ICCAD)*. IEEE, 131–138.
 - [27] Christoph Molnar. 2020. *Interpretable machine learning*. Lulu. com.
 - [28] Puja Mondal, Supriya Adhikary, Suparna Kundu, and Angshuman Karmakar. 2024. ZKFault: Fault attack analysis on zero-knowledge based post-quantum digital signature schemes. In *International Conference on the Theory and Application of Cryptology and Information Security*. Springer, 132–167.
 - [29] Kit Murdoch, David Oswald, Flavio D. Garcia, Jo Van Bulck, Daniel Gruss, and Frank Piessens. 2020. Plundervolt: Software-based Fault Injection Attacks against Intel SGX. In *Proceedings of the 41st IEEE Symposium on Security and Privacy (S&P'20)*.
 - [30] Onur Mutlu and Jeremie S Kim. 2019. Rowhammer: A retrospective. *IEEE Transactions on Computer-Aided Design of Integrated Circuits and Systems* 39, 8 (2019), 1555–1571.
 - [31] Jon Nordby, Mark Cooke, and Adam Horvath. 2019. emlearn: Machine Learning inference engine for Microcontrollers and Embedded Devices. doi:10.5281/zenodo.2589394
 - [32] Abdullah Caglar Oksuz, Anisa Halimi, and Erman Ayday. 2024. AUTOLYCUS: Exploiting Explainable Artificial Intelligence (XAI) for Model Extraction Attacks against Interpretable Models. *Proceedings on Privacy Enhancing Technologies* (2024).
 - [33] P. Qiu, D. Wang, Y. Lyu, and G. Qu. 2019. VoltJockey: Breaking SGX by Software-Controlled Voltage-Induced Hardware Faults. In *AsianHOST '19*. 1–6.
 - [34] J Ross Quinlan. 2014. *C4. 5: programs for machine learning*. Elsevier.
 - [35] Adnan Siraj Rakin, Md Hafizul Islam Chowdhury, Fan Yao, and Deliang Fan. 2022. Deepsteal: Advanced model extractions leveraging efficient weight stealing in memories. In *2022 IEEE symposium on security and privacy (SP)*. IEEE, 1157–1174.
 - [36] Reza Shokri, Marco Stronati, Congzheng Song, and Vitaly Shmatikov. 2017. Membership inference attacks against machine learning models. In *2017 IEEE symposium on security and privacy (SP)*. IEEE, 3–18.
 - [37] Mai Shouman, Tim Turner, and Rob Stocker. 2011. Using Decision Tree for Diagnosing Heart Disease Patients. *AusDM* 11 (2011), 23–30.
 - [38] Dilara Toprakhisar, Svetla Nikova, and Ventzislav Nikov. 2024. SoK: Parameterization of Fault Adversary Models Connecting Theory and Practice. In *Cryptographers' Track at the RSA Conference*. Springer, 433–459.
 - [39] Florian Tramèr, Fan Zhang, Ari Juels, Michael K Reiter, and Thomas Ristenpart. 2016. Stealing machine learning models via prediction {APIs}. In *25th USENIX security symposium (USENIX Security 16)*. 601–618.
 - [40] Michael Tunstall, Debdeep Mukhopadhyay, and Subidh Ali. 2011. Differential fault analysis of the advanced encryption standard using a single fault. In *IFIP international workshop on information security theory and practices*. Springer, 224–233.
 - [41] Jasper Van Woudenberg and Colin O'Flynn. 2021. *The hardware hacking handbook: breaking embedded security with hardware attacks*. No Starch Press.
 - [42] Jiesheng Wei, Anna Thomas, Guanpeng Li, and Karthik Pattabiraman. 2014. Quantifying the accuracy of high-level fault injection techniques for hardware faults. In *2014 44th Annual IEEE/IFIP International Conference on Dependable Systems and Networks*. IEEE, 375–382.
 - [43] Bang Wu, Xiangwen Yang, Shirui Pan, and Xingliang Yuan. 2022. Model extraction attacks on graph neural networks: Taxonomy and realisation. In *Proceedings of the 2022 ACM on Asia conference on computer and communications security*. 337–350.